Red fluorescent nanoprobe based on Ag@Au nanoparticles and graphene quantum dots for H_2O_2 determination and living cell imaging

Ling-Ling Shang[1] · Xiaojie Song[1] · Chang-Bin Niu[1] · Qi-Yan Lv[1] · Chun-Ling Li[1] · Hui-Fang Cui[1] · Shoutao Zhang[1]

Abstract

A sensitive and turn-on fluorescence nanoprobe based on core-shell Ag@Au nanoparticles (Ag@AuNPs) as a fluorescence receptor and red emissive graphene quantum dots (GQDs) as a donor was fabricated. They were conjugated together through π-π stacking between the GQDs and single-strand DNA modified at the Ag@AuNPs surface. The absorption spectrum of the receptor significantly overlapped with the donor emission spectrum, leading to a strong Förster resonance energy transfer (FRET) and thus a dramatic quenching. The sensing mechanism relies on fluorescence recovery following DNA cleavage by •OH produced from Fenton-like reaction between the peroxidase-like Ag nanocore and H_2O_2. The red emissive feature (Ex/Em, 520 nm/560 nm) provides low background in physiological samples. The •OH production, great spectrum overlapping, and red emission together contributes to good sensitivity and living cell imaging capability. The fluorescence assay (intensity at 560 nm) achieves a low detection limit of 0.49 μM H_2O_2 and a wide linear range from 5 to 200 μM, superior to most of the reported fluorescent probes. The RSD value for 100 μM H_2O_2 was 1.4%. The nanoprobe exhibits excellent anti-interferences and shows low cytotoxicity. The recovery of 100 μM standard H_2O_2 in a cancer cell lysate was 85.8%. Most satisfactorily, it can realize monitoring and imaging H_2O_2 in living cells. This study not only presents a sensitive H_2O_2 probe but also provides a platform for detecting other types of reactive oxygen species.

Introduction

H_2O_2, one of the reactive oxygen species (ROS), is important in biomedical processes, including cell proliferation, differentiation, and migration [1]. However, disorder of H_2O_2 leads to various diseases such as cancer and central nervous system diseases [2]. In addition to H_2O_2,

various other ROS, including hydroxyl radicals (•OH) and superoxide ions ($O_2\bullet^-$), are generated as results of oxidative metabolism in a variety of physiological and pathological activities [3]. Therefore, the detection of H_2O_2 and other physiological ROS is crucial for clinical diagnosis and biomedical research. Evidence has shown that several types of tumor cells generate more H_2O_2 than their normal counterparts and normal tissues, originating from the abnormal growth of the tumor [4]. H_2O_2 is dangerous to human health and life when its concentration exceeds to 75 ppm (i.e. 2.2 mM) [5]. Traditional detection methods for H_2O_2 include titration and chromatography methods. While titration is limited by its low sensitivity, both of the methods cannot realize in situ and real-time H_2O_2 measurement. Additionally, chromatography suffers from the drawback of high instrument cost. Thus, a sensitive, accurate, and in situ method to detect H_2O_2 is urgently expected.

Ling-Ling Shang and Xiaojie Song contributed equally to this work.

This article is part of the Topical Collection on *Nanomaterials for biomedical imaging and targeting*

✉ Hui-Fang Cui
hfcui@zzu.edu.cn

1 School of Life Sciences, Zhengzhou University, 100# Science Avenue, Zhengzhou 450001, China

Until now, a number of methods for H_2O_2 detection have been reported, such as electrochemistry, spectrophotometry, chemiluminescence, fluorescence, and colorimetric method [6]. However, some of the methods still cannot realize in situ H_2O_2 detection. Fortunately, fluorescent probes show convenience, high specificity, and sensitivity for in situ measuring endogenous H_2O_2 in living cells [7]. In recent years, some turn-on fluorescent probes based on Förster resonance energy transfer (FRET) have attracted great interests [8]. In FRET, fluorescence donor is quenched by fluorescence receptor when the distance between them is less than 10 nm [9]. In the presence of H_2O_2, fluorescence recovers when the FRET system cracks. Therefore, the fluorescence recovery intensity can be used for H_2O_2 detection. However, low biocompatibility, high photobleaching (like organic fluorophores), biological matrix autofluorescence interference, and low sensitivity are the major barriers for wide application of FRET fluorescent probes in biological systems.

In FRET system, the absorption spectrum of fluorescence receptor should greatly overlap with the donor emission spectrum, to result in a dramatic quenching effect and, therefore, a low fluorescence background. Silver nanoparticles (AgNPs) have unique and tunable optical properties, benefiting from their strong localized plasmon resonance (SPR) feature. They have been validated as a good FRET receptor in an AgNPs/graphene quantum dots (GQDs) hybrid nanoprobe [10]. A H_2O_2 fluorescent probe was fabricated by coupling the fluorescence receptor and the fluorescence donor (i.e., GQDs) through π-π stacking between the GQDs and single-strand DNA molecules modified at the AgNPs surface [11]. AgNPs possess peroxidase-like activity, capable of reacting with H_2O_2, producing hydroxyl radical (•OH) [12]. Upon H_2O_2 addition, the DNA strand was cleaved by the •OH produced from the Fenton-like reaction [11]. Nevertheless, AgNPs are unstable and oxidative, especially in acidic conditions [11, 12]. In contrast, it is well-known that gold is resistant to oxidation and has beneficial reactivity with sulfur component such as DNA-SH (DNA with a –SH moiety). However, gold nanoparticles (AuNPs) do not have peroxidase-like activity and cannot react with H_2O_2.

In order to take advantages of both AgNPs and AuNPs in a single nanoprobe, silver and gold were coupled as a core-shell nanostructure with enhanced optical properties and oxidation resistance ability [13]. Moreover, the optical properties of the Ag@Au core-shell nanoparticles (Ag@AuNPs) can be tuned to cover the entire visible to near-infrared (NIR) region by changing the size of Ag core and the thickness of Au shell [14]. The unique properties of Ag@AuNPs inspired us to design and search a desirable fluorescence donor, which emission spectrum greatly overlaps with the tunable absorption spectrum of Ag@AuNPs, to construct a novel, sensitive, and turn-on fluorescent H_2O_2 nanoprobe.

Carbon dots (CDs) as a FRET donor have advantages of high water solubility, biocompatibility, eco-friendliness, and good fluorescence quantum yield [15, 16]. They have been used for cell imaging [17–19]. Particularly, graphene quantum dots (GQDs), one specific type of CDs, exhibit unique optical and electronic properties due to their quantum confinement and edge effects [20]. GQDs possess carboxyl and hydroxyl groups, large surface-to-volume ratio, low cytotoxicity, and good electrical conductivity. Hence, GQDs have shown a variety of applications in biological imaging, optical sensor, drug delivery, and biosensing, etc. [21]. However, a majority of CDs probes are green or blue fluorescent, suffering from strong matrix autofluorescence interference and low sensitivity [22]. Development of sensitive fluorescent probes based on near-infrared emission or red emission GQDs has aroused scientists' interests. To our knowledge, a H_2O_2 detection nanoprobe constructed from red emissive GQDs has not been reported.

In this study, a turn-on, red fluorescent H_2O_2 nanoprobe based on Ag@AuNPs and red emissive GQDs as FRET receptor and donor, respectively, was fabricated. The tunable absorption of Ag@AuNPs makes the Ag@AuNPs and red emissive GQDs a great FRET receptor-donor pair, which has not been reported to our knowledge. Herein, Ag@AuNPs were prepared and tuned to a desirable SPR, red emissive GQDs were prepared and characterized, and single-strand DNA was modified on the surface of Ag@AuNPs through Au-S covalent bond. GQDs as a signal output unit were then assembled on the surface of the DNA-decorated Ag@AuNPs through π-π stacking to fabricate an Ag@AuNPs-DNA/GQDs nanoprobe (Scheme 1). This nanoprobe achieves fluorescence recovery through DNA cleavage by •OH, which can be massively produced by a Fenton-like reaction between the Ag nanocore and H_2O_2. Under optimum conditions, the fabricated nanoprobes showed superior performances including low detection limit, wide linear range, anti-interference ability, and low cytotoxicity. Most importantly, H_2O_2 level in living cells can be monitored in situ with fluorescence imaging. In a short, a convenient and sensitive fluorescent nanoprobe for H_2O_2 detection and living cell imaging was designed and fabricated, which holds a great potential for applications in biomedical research, clinical diagnosis, and pharmaceutical and environmental detection.

Experimental

Chemicals and reagents

Gold chloride trihydrate (purity ≥99.9%), citric acid monohydrate, hydrogen peroxide, urea, and ethylenediaminetetraacetic acid (EDTA), etc. were purchased from Sinopharm Chemical Reagent Co., Ltd. (Shanghai, China). Hoechst

Scheme 1 Schematic diagram of the construction process of Ag@AuNPs-DNA/GQDs fluorescent probe and the mechanisms for H_2O_2 detection and living cell imaging
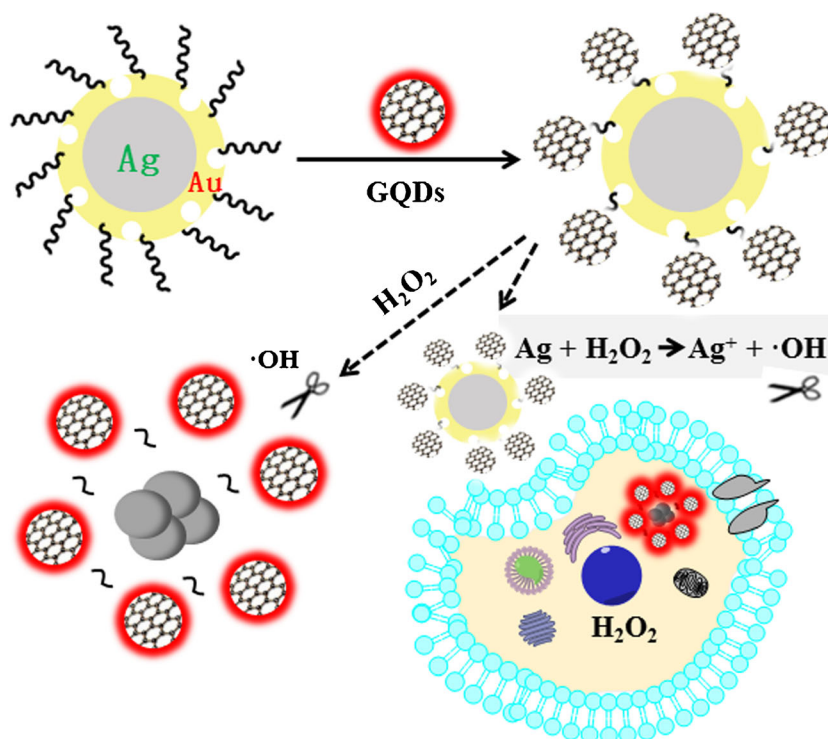
33342, 3,3′,3″-phosphinetriyltripropanoic acid (TCEP), sodium borohydride, and dimethyl sulfoxide (DMSO) were supplied by Sigma-Aldrich (USA). Dulbecco's Modified Eagle Medium (DMEM, high glucose), 1640 medium, 1× PBS, trypsin (0.25%), tris (hydroxymethyl) aminomethane, and thiazolyl blue tetrazolium bromide (MTT) were purchased from Solarbio Life Science Co., Ltd. (Beijing, China). Fetal bovine serum (FBS) was obtained from Gbico Co. (USA). ROS agent (Rosup) was purchased from Beyotime Biotechnology Co., Ltd. (Shanghai, China). The 2′,7′-dichlorodihydrofluorescein diacetate (H2DCFDA, short name: HDCF) dye was obtained from Hawn Chemical Reagent Co. (Shanghai, China). SH-DNA: 5′-SH-(CH₂)₆-ATA CCA ATA TCC GCT TTA-3′ was synthesized and purified by Sangon Biotech Co., Ltd. (Shanghai, China). All other chemicals were of analytical grade. Deionized water ($\geq$ 18 MΩ cm) was obtained from a Millipore water system and used throughout the experiment.

Instruments and characterizations

GQDs were synthesized in a SX-G12123 muffle (Zhong Huan, Tianjin, China). UV-vis spectrometry was performed on UV-vis spectrophotometer UV-2600 (Shimadzu, Japan). Fluorescence spectroscopy was performed using spectrofluorometer F-4500FL (Hitachi, Japan). Fourier transform infrared (FTIR) spectra were collected using PerkinElmer Spectrum 2 FTIR spectrophotometer. The material morphologies were observed on JEM-2800 Transmission Electron Microscope

(TEM, JEOL, Japan). The X-ray photoelectron spectroscopy (XPS) spectra of GQDs were detected by AXIS Supra detector (Shimadzu, Japan). The element mapping of Ag@AuNPs was measured by using an Oxford XMax-80 T Energy Dispersive System (EDS) detector. Cells were cultured in a HF160W incubator of Heal Force. Cell cytotoxicity of the Ag@AuNPs-DNA/GQDs probe was measured using a Microplate Reader (EMax Plus, Medidata, USA). The cell fluorescence images were collected on a confocal laser scanning microscopy (CLSM) (Zeiss LSM880, Germany).

Preparation of GQDs and Ag@AuNPs

The red emissive GQDs were synthesized according to the reported hydrothermal method [23] with some modifications. The Ag@AuNPs were synthesized according to the reported synthetic method for hollow Au nanoparticles [14], with controlling the added HAuCl₄ solution volume and monitoring the SPR peak of the reaction mixture. The detailed preparation processes are described in Supplementary Materials.

Fabrication of the Ag@AuNPs-DNA/GQDs nanoprobe

To fabricate the nanoprobe, the SH-DNA was firstly coupled on the Ag@AuNPs surface through formation of Au-S bounds, producing Ag@AuNPs-DNA nanocomplex. The SH-DNA sequence was designed to be 5′-SH-(CH₂)₆-ATA CCA ATA TCC GCT TTA-3′ because it does not tend to form secondary structure and the length is less than 10 nm, which is

suitable for FRET quenching between GQDs and Ag@Au NPs. Briefly, the AgNPs solution (500 μL 200 μg·mL^{-1}) was added into 65 μL 1 μM SH-DNA, which was pretreated with TCEP to reduce disulfide bond. The mixture was stirred at room temperature for 16 h. Afterwards, it was centrifuged at 12000 rpm for 10 min. The precipitate was washed and then dispersed in 10 mM pH 7.4 PBS buffer, resulting in the Ag@AuNPs-DNA solution. Then, GQDs were assembled on the surface of the Ag@AuNPs-DNA nanocomplex through π-π stacking. To facilitate the π-π stacking, the Ag@AuNPs-DNA solution (300 μL 50 μg·mL^{-1}) was added into 550 μL 15 μg·mL^{-1} GQDs solution, and the mixture was incubated at room temperature for 5 h. Finally, the Ag@AuNPs-DNA/GQDs nanoprobe was washed twice under centrifugation at 12000 rpm for 10 min to remove redundant GQDs and then dispersed in pH 7.4 PBS, ready for use.

In optimization of the fabrication conditions, the SH-DNA concentration, GQDs concentration, and the incubation time between the Ag@AuNPs-DNA and the GQDs were varied (detailed in Supplementary Materials), and the H$_2$O$_2$ response signal intensities of the corresponding nanoprobes were evaluated.

H$_2$O$_2$ detection and sensing performances

In detection of H$_2$O$_2$, a 5 μL H$_2$O$_2$ solution or sample was added into the nanoprobe solution (550 μL 92 μg·mL^{-1}), and then the mixture was incubated at 37 °C for 2 h. For unknown samples, for example, a cell lysate, the sample was centrifuged at 1000 rpm before detection, and the supernatant was collected. The fluorescence intensities before and after the H$_2$O$_2$ solution or the sample was added were recorded as F$_0$ and F, respectively. In the fluorescence measurement, the excitation was set at 520 nm, and the PMT was 700 V. The fluorescence emission intensity was acquired at 560 nm. The value of F-F$_0$ was referred as fluorescence recovery. The fluorescence ratio of F/F$_0$ was taken as the H$_2$O$_2$ response signal. To optimize the response time, a 100 μM H$_2$O$_2$ solution was incubated with the nanoprobe for various periods (varied from 1 to 3 h), and the H$_2$O$_2$ response signal intensities were compared.

To evaluate the detection sensitivity and the dynamic range, a series of various concentrations of H$_2$O$_2$ were detected, and the plot of F/F$_0$ versus H$_2$O$_2$ concentration was drawn. In order to investigate the H$_2$O$_2$ detection specificity, various interfering compounds such as glucose (Glu), human serum albumin (HSA), ascorbic acid (AA), NaCl, CaCl$_2$, MgCl$_2$, and FeCl$_3$ were detected with the nanoprobe. The interferents concentrations were chosen based on their physiological levels (Supplementary Materials). In addition, to evaluate the matrix effect of physiological samples, we spiked 100 μM H$_2$O$_2$ into a MCF-7 cell lysate (the protein concentration of the lysate was determined to be 0.128 mg mL^{-1}, by using BCA Protein Assay kits). The H$_2$O$_2$ detection recovery rate (found level/

known level) was determined. Furthermore, the nanoprobe was stored in sterilized PBS (pH = 7.4) at 4 °C to assess its storage stability.

Fluorescence imaging of H$_2$O$_2$ in living cells

To investigate the H$_2$O$_2$ imaging performance of the Ag@AuNPs-DNA/GQDs nanoprobe in living cells, human embryonic kidney cells (HEK-293 T cells) and breast cancer cells (MCF-7 cells) were cultured. Before the H$_2$O$_2$ imaging was conducted, the cytotoxicity of the nanoprobe was investigated through MTT assay firstly. The cell culture and the MTT assay procedures are described in the Supplementary Materials. In H$_2$O$_2$ imaging, the HEK-293 T cells and MCF-7 cells were seeded in 35-mm dishes at a density of 3.0×10^5 cells/dish and incubated to about 80% cell confluence. Subsequently, the medium was replaced with 1 mL fresh medium containing with or without 30 μg·mL^{-1} Ag@AuNPs-DNA/GQDs. As an ROS positive control, 1 μL 50 μg mL^{-1} Rosup was added to the Ag@AuNPs-DNA/GQDs pretreated cell culture and incubated for 20 min. After 4 h of nanoprobe incubation, cells were washed with PBS thrice, followed by addition of Hoechst (1 mL 10 μg·mL^{-1}) and then incubation for 15 min. In addition, a commercial cellular H$_2$O$_2$ probe HDCF (10 μM) was applied and cultured with the cells for 30 min, instead of the Ag@AuNPs-DNA/GQDs nanoprobe, to evaluate the nanoprobe performances in living cell imaging. Then cells were washed with PBS and observed under CLSM with oil objective at collection range of 450 ~ 490 nm or 500 ~ 570 nm (excited at 405 nm or 480 nm, respectively). Fluorescence intensities of the CLSM images were semi-quantified through Zeiss Zen 3.2.

Results and discussion

Characterization of GQDs, Ag@AuNPs, and Ag@AuNPs-DNA

The GQDs are spherical particles with 3.2–4.8 nm in diameter (Fig. 1a). They have crystalline carbon structure with the lattice fringe distance of 0.21 nm, attributed to the d spacing of graphene (100) planes [23] (inset in Fig. 1a). The maximum emission is maintained at about 580 nm when the excitation wavelength increased to ≥520 nm (Fig. S-1a). In addition, the XPS spectra of GQDs suggest that the GQDs possess -OH, -COOH, C-C, C=C, C-N, and -C=O groups [23] (Fig. S-1(b-f)). The GQDs with obvious graphene lattice should be able to interact with the DNA strands on Ag@AuNPs though π-π stacking, feasible for fabrication of the designed nanoprobe.

In synthesis of Ag@AuNPs, with the gradual addition of the HAuCl$_4$ solution, the reaction mixture gradually changed from yellow, yellow-gray, to gray (Fig. S-2a). Meanwhile, the

Fig. 1 **a** TEM images of the GQDs. **b** Uv-vis spectrum of the Ag@AuNPs and fluorescence spectrum of the GQDs. **c** TEM images of the Ag@AuNPs. **d** Uv-vis spectra of Ag@AuNPs without and with DNA modification. The two insets in (**a**) and (**c**) show size distribution and HRTEM, respectively
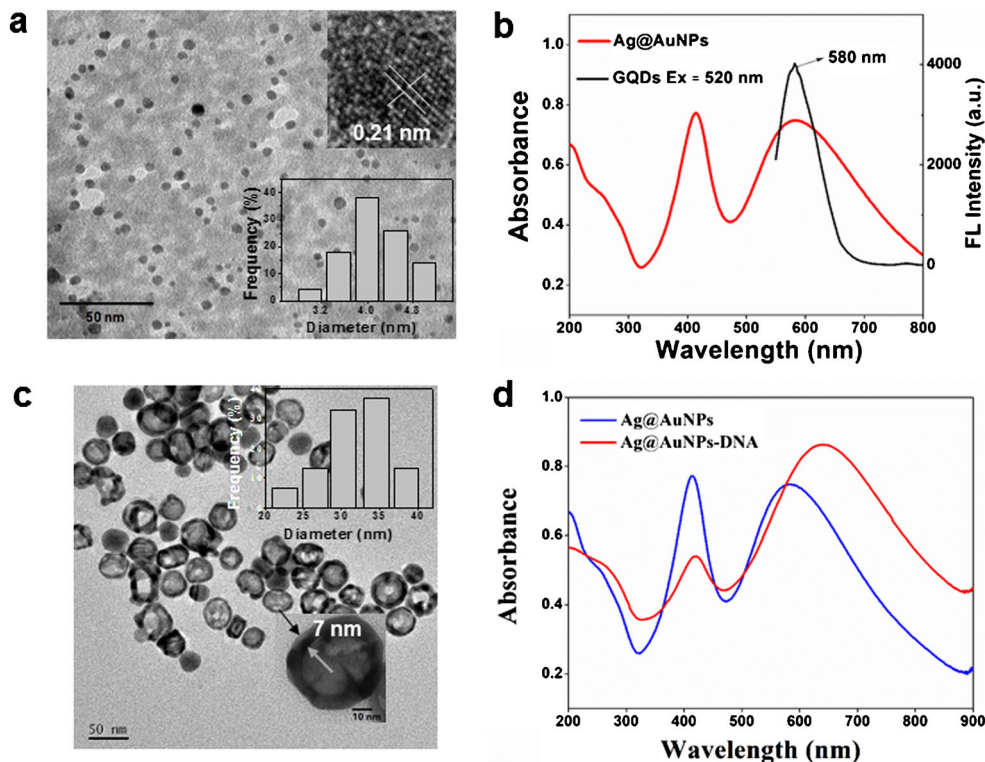
SPR peak intensity of the AgNPs at ~400 nm gradually decreased and red shifted, accompanied by a gradual appearance of an SPR peak at ~580 nm (Fig. S-2b). The absorption at ~580 nm is assigned to the SPR of the Au shell. The reaction was then stopped, as the absorption peak at ~580 nm is desired in order to greatly overlap with the emission spectrum of the red emissive GQDs (Fig. 1b). The Ag@AuNPs are spherical with a core-shell structure, and the average particle size is about 31.7 nm (Fig. 1c). This size can facilitate cell endocytosis [24]. The Au shell thickness is ~7 nm (pointed with arrows in inset in Fig. 1c). Moreover, the Ag element content in the Ag@AuNPs was measured to be 48.15% (wt%) by EDS analysis (Fig. S-2c), confirming the existence of the Ag nanocore. The Ag nanocore would allow the nanoprobe react with H_2O_2 following a Fenton-like reaction, producing massive •OH radical.

To couple GQDs with AgNPs, DNA-SH was conjugated on the Ag@AuNPs surface through Au-S bond. After DNA modification (Fig. 1d), DNA absorption at 260 nm appeared, and the SPR peak of the Au shell shifts from 580 to 650 nm because of refractive index changes [25]. Moreover, some characteristic peaks of DNA appear in the FTIR spectrum (Fig. S-2d). All the results indicate that DNA strands have been successfully conjugated on the surface of Ag@AuNPs.

Feasibility of the Ag@AuNPs-DNA/GQDs nanoprobe

Firstly, to verify the feasibility of the nanoprobe design principle, the Ag@AuNPs-DNA solution was increasingly added into the GQDs solution, and the fluorescence spectroscopy was monitored. It was observed that the fluorescence intensity of the GQDs at ~580 nm gradually decreased with the Ag@AuNPs-DNA titration (Fig. S-3A). When the Ag@AuNPs-DNA concentration reached 100 µg·mL^{-1}, a quenching efficiency of 90% was attained. In contrast, titration of Ag@AuNPs (DNA-unmodified) into the GQDs solution resulted in a significantly smaller quenching efficiency, in comparison to Ag@AuNPs-DNA (Fig. S-3B). The result suggests that the fluorescence of GQDs can be quenched effectively by Ag@AuNPs-DNA due to FRET effect. The effective FRET is contributed by the great overlapping between the GQDs fluorescence spectrum and the Ag@AuNPs-DNA absorption spectrum and a π-π stacking between the purine or pyrimidine bases of DNA and the graphene planes of GQDs. Then, the Ag@AuNPs-DNA/GQDs conjugates were subject to TEM analysis (Fig. 2a) and fluorescence measurement (Fig. 2b). The TEM image shows that the Ag@AuNPs-DNA/ GQDs are satellite-like nanocomplexes with multiple GQDs surrounding Ag@AuNPs (Fig. 2a). The DNA molecules of Ag@AuNPs-DNA can conjugate to the surface of GQDs through π-π stacking. The successful conjugation of the GQDs on Ag@AuNPs-DNA resulted in a dramatic quenching of the GQDs fluorescence in the Ag@AuNPs-DNA/GQDs nanoprobe (Fig. 2b). In response to 100 µM H_2O_2, the fluorescence recovers to a great extent (Fig. 2b), suggesting efficient cleavage of the single-strand DNA. It has been reported that AgNPs can react with H_2O_2 following Fenton-like

Fig. 2 **a** TEM image of the Ag@AuNPs-DNA/GQDs nanoprobe; **b** fluorescence spectra of the Ag@AuNPs-DNA/GQDs nanoprobe without and with incubation with 100 μM H_2O_2. The arrows in (**a**) point to some of the GQDs surrounding the Ag@AuNPs
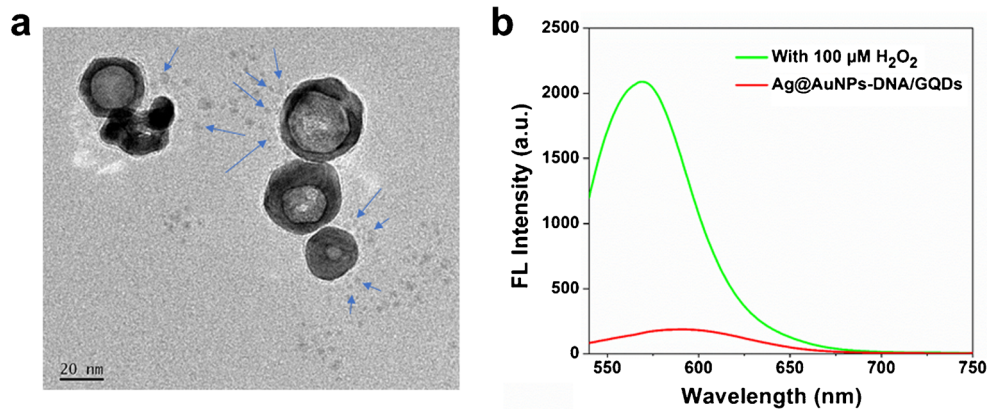
reaction, producing •OH, especially in acidic media [12]. The •OH can cleave DNA molecules [11]. To investigate the H_2O_2 response mechanism underling the Ag@AuNPs-DNA/GQDs nanoprobe, we added ROS scavengers isopropanol (IPA) or L-Cysteine (L-Cys), together with H_2O_2 to the Ag@AuNPs-DNA/GQDs nanoprobe. IPA and L-Cys are the scavengers of •OH and almost all ROS, respectively [26]. When 1.0 mM IPA or 1.0 mM L-Cys was added, the florescence recovery was completely suppressed (Fig. S-4). The results indicate that ROS, mainly •OH, is produced and functions as DNA cleaving agent in the nanoprobe system, confirming that the Ag@AuNPs can react with H_2O_2 following a Fenton-like reaction. This result is consistent with a study reporting that AgNPs react with H_2O_2 and produce •OH [12]. In addition, to investigate the effect of Ag nanocore etching on fluorescence recovery, we introduced NaClO into the Ag@AuNPs-DNA/GQDs nanoprobe instead of H_2O_2. NaClO has a slightly higher redox potential than H_2O_2 and therefore can exhibit a slightly stronger etching ability to the Ag nanocore. It was found that NaClO cannot lead to stronger florescence recovery than the blank (Fig. S-5), excluding any positive effect of Ag nanocore etching on the nanoprobe working. In fact, it was found that NaClO decreased the fluorescence of the nanoprobe system in comparison to the blank buffer. The exact reason is unknown at this moment, probably because NaClO can inhibit the fluorescence of GQDs.

Optimization and H_2O_2 sensing performances

Then the conditions in the nanoprobe fabrication and H_2O_2 detection were optimized (Fig. S-6). Furthermore, the detection sensitivity and linearity of the nanoprobe in detecting H_2O_2 was evaluated. Figure 3A illustrates the fluorescence spectra in detecting a series of different concentrations of H_2O_2. The fluorescence intensity increased monotonically with the H_2O_2 concentration from 5 to 200 μM, with a semi-log linear calibration equation of $F/F_0 = 0.86 + 4.19 \times lgC(H_2O_2)$ (μM) (inset in Fig. 3A). The linear regression coefficient is 0.9973, with a limit of detection (LOD) of

0.49 μM. The LOD value was estimated following the 3σ rule of 3 times standard deviation (SD) over the blank response. The LOD value and the linear range are comparable to or better than those of other nanoprobes published for H_2O_2 detection (Table 1) [11, 27–30]. In addition, the nanoprobe is very reproducible, with an RSD value of 1.4% for detecting 100 μM H_2O_2. The excellent sensitivity should be attributed to the following factors: (1) the core-shell Ag@AuNPs can dramatically quench the red fluorescence of GQDs, resulting in a very low background; (2) massive •OH radicals can be generated from the Fenton-like reaction between the Ag@AuNPs and H_2O_2, effectively cleaving the DNA strands. Moreover, the nanosize, red fluorescent, and stable Au shell should make the Ag@AuNPs-DNA/GQDs nanoprobe superior in biological imaging. Due to irradiation and matrix autofluorescence, blue or green fluorescent probes can cause damage to biological systems and have high matrix background. The performances of the nanoprobe on anti-interference ability, recovery in biological samples, storage stability, and living cell imaging were then assessed.

Possible interfering species including glucose, protein, AA, and various metal ions were detected with the nanoprobe. Except for a very strong signal to the H_2O_2 target, none of the interfering species resulted in obvious signal responses (Fig. 3B). In addition, to evaluate the matrix effect of physiological samples to the nanoprobe, 100 μM H_2O_2 was spiked into the MCF-7 cell lysate. The endogenous H_2O_2 level in the cell lysate was measured to be 5.42 μM, and the recovery rate of the spiked H_2O_2 was 85.8%. The results indicate that the nanoprobe can selectively detect H_2O_2. Cell lysate has very slight matrix effect to nanoprobe. After storing at 4 °C for 7, 14, and 21 days, the detection signals of the nanoprobe towards 100 μM H_2O_2 retained 93.3%, 82.8%, and 71.7% intensity, respectively, compared to freshly prepared nanoprobe. The storage stability values are acceptable. To our knowledge, almost no storage stability values for fluorescent nanoprobes were reported. The slightly lost signal after the storage is contributed both by a slight dissociation of GQDs and a decrease of the intrinsic fluorescence of the GQDs. We found that, although the GQDs were stable at dry
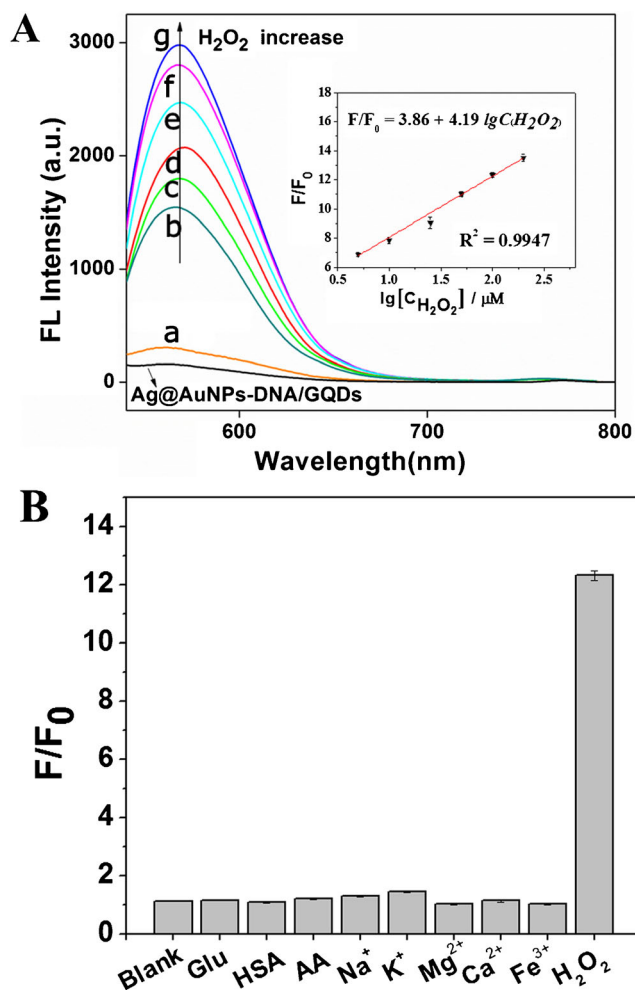
Fig. 3 (A) Fluorescence emission spectra of the Ag@AuNPs-DNA/GQDs nanoprobe without and with incubation with various concentrations of H_2O_2 (from curve "a" to curve "g," the H_2O_2 concentration was 0, 5, 10, 25, 50, 100, and 200 μM, respectively). The inset stands for the plot of F/F_0 versus the H_2O_2 concentration, where F_0 and F are the fluorescence intensity of the probe at 560 nm without and with incubation with a H_2O_2 solution, respectively. (B) Anti-interference ability of the nanoprobe for H_2O_2 detection (100 μM H_2O_2). The interferences tested include 8 mM Glu, 50 mg·mL^{-1} HSA, 20 μg·mL^{-1} AA, 154 mM NaCl, 4 mM KCl, 1.5 mM CaCl$_2$, 1.3 mM MgCl$_2$, or 32 μM FeCl$_3$

in vacuum, their fluorescence intensity decreased in solution. Improvement on the synthesis method for GQDs is still an important and challenging task.

Cytotoxicity and fluorescence imaging in living cells

The cytotoxicity of the Ag@AuNPs-DNA/GQDs probe is shown in Fig. S-7. The survival rates of both MCF-7 cells and HEK-293 T cells were more than 80% when the probe concentrations were less than 50 μg·mL^{-1}, suggesting that the nanoprobe has a negligible effect on cellular viability. For living cell imaging, both MCF-7 cells and HEK-293 T cells were used. The images of MCF-7 cells and HEK-293 T cells are shown in Fig. 4 and Fig. S-8a, respectively. For MCF-7 cells, significant enhancement of red fluorescence in the cytoplasm around the blue nucleus was observed with the nanoprobe incubation (Fig. 4, Fig. S-8b). The results indicate that the Ag@AuNPs-DNA/GQDs have been taken up by the cells and responded to endogenous H_2O_2 [7]. Upon addition of the ROS agent Rosup together with the nanoprobe, significantly stronger red emission was observed (Fig. 4, Fig. S-8b). Rosup is a ROS agent that can induce ROS production in living cells. The commercial H_2O_2 probe HDCF showed similar results with the Ag@AuNPs-DNA/GQDs nanoprobe, exhibiting stronger green fluorescence with the Rosup introduction. Rosup elevates the oxidative stress and the ROS level in the cells, which are captured and detected by the nanoprobe.

In contrast, no obvious red fluorescence in HEK-293 T cells was observed with the nanoprobe incubation (Fig. S-8a). In addition, the fluorescence intensity of the nanoprobe in HEK-293 T cells was significantly smaller than that in the MCF-7 cells (Fig. S-8b). These results prove that the H_2O_2 or ROS level in the MCF-7 cancer cells is obviously higher than that in the HEK-293 T normal cells. It is well known that most cancer cells exhibit elevated endogenous ROS and H_2O_2 levels [31, 32]. With the addition of the ROS agent Rosup, a significantly stronger red emission in the HEK-293 T cells was induced by the nanoprobe (Fig. S-8a and S-8b), similar to the MCF-7 cells. Again, the imaging results of the nanoprobe are consistent with the commercial probe HDCF.

The above results indicate that the nanoprobe has living cell imaging capability to differentiate the H_2O_2 or ROS levels in cancer cells from those in normal cells and detect endogenous and exogenous H_2O_2 or ROS levels. The living cell imaging capability is attributed to the red emissive feature and the nanosize of the nanoprobe, which can result in low physiological background and efficient cell endocytosis.

Table 1 Comparisons with some other nanoprobes published for H_2O_2 detection

Probe	Linear range (μM)	Detection limit (μM)	Ref.
AgNP-DNA@GQDs	2.0–100	0.42	[11]
Eu(III)-MOF	2.0–200	1.02	[27]
C-dots	0.5–100	0.25	[28]
T-CuNPs	0.55–110	0.55	[29]
N-CQDs/TMB	100–500	35.0	[30]
Ag@AuNPs-DNA/GQDs	5–200	0.49	**This work**

Fig. 4 Fluorescence images of MCF-7 cells after being incubated with 30 $\mu g \cdot mL^{-1}$ Ag@AuNPs-DNA/GQDs for 4 h. The groups of control, nanoprobe, Rosup, Rosup + nanoprobe, HDCF, and Rosup + HDCF are the cells treated with the culture media without other additives or with the addition of nanoprobe, Rosup, Rosup + nanoprobe, HDCF, and Rosup + HDCF, respectively. The bright field, blue, red, green, and merge images are the images observed at bright field channel, fluorescence from Hoechst, fluorescence from GQDs, fluorescence from HDCF, and merge of the above, respectively. Scale bar denotes 10 μm
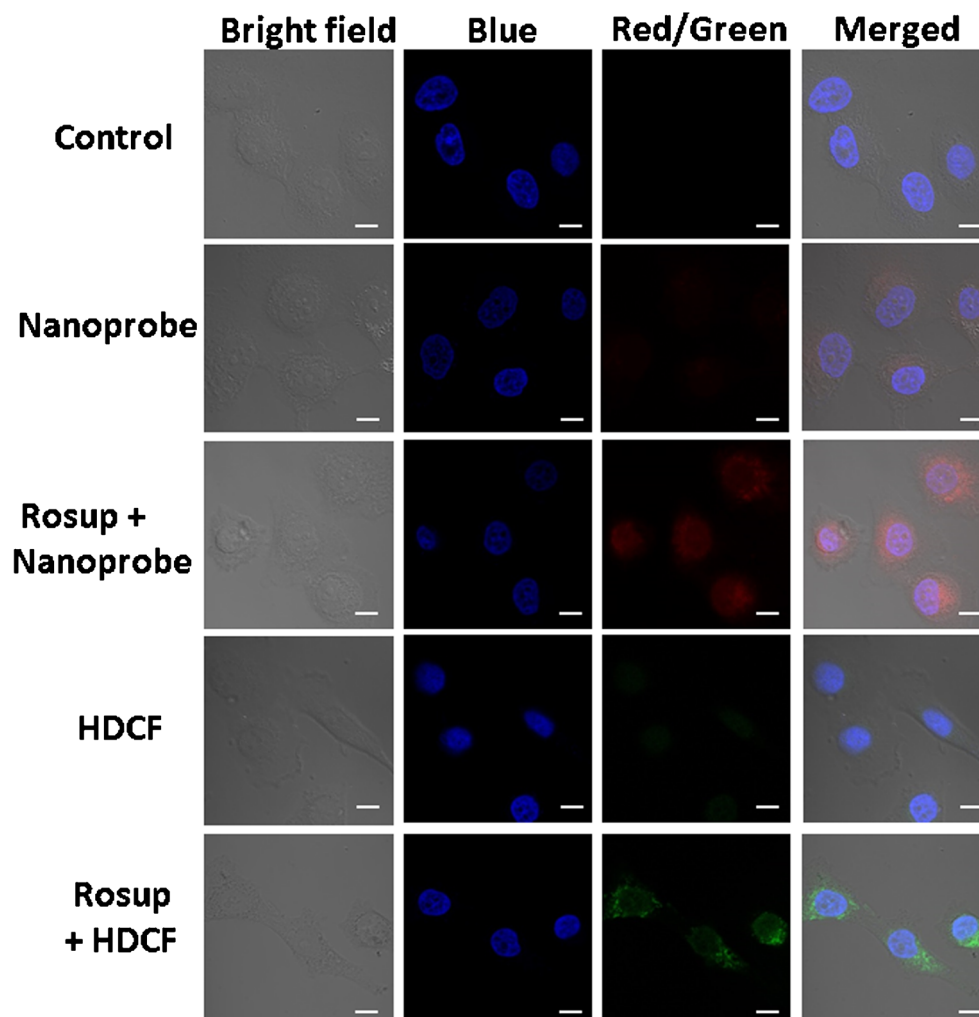
Overall, the Ag@AuNPs-DNA/GQDs nanoprobe is biocompatible to cells. By using the Ag@AuNPs-DNA/GQDs nanoprobe, red fluorescent, in situ, and real-time imaging of H_2O_2 in living cells have been realized. The storage stability of the nanoprobe is not very ideal but acceptable, which has been seldom reported for other fluorescent nanoprobes. Improvement on the synthesis of GQDs is still an important and challenging task.

Conclusions

A sensitive fluorescence nanoprobe based on FRET mechanism for H_2O_2 detection has been fabricated. With the specially designed and synthesized core-shell Ag@AuNPs, the fluorescence of GQDs can be quenched by Ag@AuNPs effectively. Through π-π stacking between the DNA strands modified on Ag@AuNPs and the GQDs, GQDs have been conjugated on Ag@AuNPs surface, forming a satellite structured nanoprobe. Attributing to the synergistic effect of red emission, excellent FRET, and effective DNA cleavage, the fluorescence nanoprobe shows high detection sensitivity towards H_2O_2. In addition, it possesses excellent anti-interference ability. More importantly, the nanoprobe has a negligible cytotoxicity and can be effectively taken up by tumor cells. Consequently, the nanoprobe has shown living cell imaging capability and can detect H_2O_2 or ROS levels in cells. In a short, a convenient and sensitive nanoprobe for H_2O_2 detection has been fabricated, which exhibits great potential for applications in biological field.

Declarations

Conflict of interest The authors declare no competing interests.

References

1. Sun LF, Ding YY, Jiang YL, Liu QY (2017) Montmorillonite-loaded ceria nanocomposites with superior peroxidase-like activity for rapid colorimetric detection of H2O2. Sens Actuators B Chem 239:848–856. https://doi.org/10.1016/j.snb.2016.08.094

2. Lin MT, Beal MF (2006) Mitochondrial dysfunction and oxidative stress in neurodegenerative diseases. Nature 443:787–795. https://doi.org/10.1038/nature05292

3. Autreaux BD, Toledano MB (2007) ROS as signalling molecules: mechanisms that generate specificity in ROS homeostasis. Nat Rev Mol Cell Biol 8:813–824. https://doi.org/10.1038/nrm2256

4. Xi J, Xie C, Zhang Y, Wang L, Xiao J, Duan XM, Ren JH, Xiao F, Wang S (2016) Pd nanoparticles decorated N-doped graphene quantum dots@N-doped carbon hollow nanospheres with high electrochemical sensing performance in cancer detection. ACS Appl Mater Interfaces 8:22563–22573. https://doi.org/10.1021/acsami.6b05561

5. Sun J, Li CY, Qi YF, Guo SL, Xue L (2016) Optimizing colorimetric assay based on V_2O_5 nanozymes for sensitive detection of H_2O_2 and glucose. Sensors 16:584. https://doi.org/10.3390/s16040584

6. Wang Z, Ju P, Zhang Y, Jiang F, Din H, Sun C (2020) $CoMoO_4$ nanobelts as efficient peroxidase mimics for the colorimetric determination of H_2O_2. Microchim Acta 187:424. https://doi.org/10.1007/s00604-020-04376-7

7. Liu J, Liang J, Wu C, Zhao YB (2019) A doubly-quenched fluorescent probe for low-background detection of mitochondrial H_2O_2. Anal Chem 91:6902–6909. https://doi.org/10.1021/acs.analchem.9b01294

8. Yuan J, Cen Y, Kong XJ, Wu S, Xia C (2015) MnO_2-nanosheet-modified upconversion nanosystem for sensitive turn-on fluorescence detection of H_2O_2 and glucose in blood. ACS Appl Mater Interfaces 7:10548–10555. https://doi.org/10.1021/acsami.5b02188

9. Selvin PR (2000) The renaissance of fluorescence resonance energy transfer. Nat Struct Biol 7:730–734. https://doi.org/10.1038/78948

10. Liu SG, Mo S, Han L, Li N, Yu YZ, Li NB, Hong HQ (2019) Oxidation etching induced dual-signal response of carbon dots/silver nanoparticles system for ratiometric optical sensing of H_2O_2 and H_2O_2-related bioanalysis. Anal Chim Acta:81–1055, 89. https://doi.org/10.1016/j.aca.2018.12.015

11. Wang L, Zheng J, Li Y, Sheng Y, Liu C (2014) AgNP-DNA@GQDs hybrid: new approach for sensitive detection of H_2O_2 and glucose via simultaneous AgNP etching and DNA cleavage. Anal Chem 86:12348–12354. https://doi.org/10.1021/ac503653c

12. He W, Zhou YT, Wamer WG, Boudreau MD, Yin JJ (2012) Mechanisms of the pH dependent generation of hydroxyl radicals and oxygen induced by Ag nanoparticles. Biomaterials 33:7547–7455. https://doi.org/10.1016/j.biomaterials.2012.06.076

13. Cui Y, Ren B, Yao JL, Gu RA, Tian ZQ (2006) Synthesis of AgcoreAushell bimetallic nanoparticles for immunoassay based on surface-enhanced Raman spectroscopy. J Phys Chem B 110:4002–4006. https://doi.org/10.1021/jp056203x

14. Li Y, He D, Tu J, Wang R, Zu C, Chen Y, Yang W, Shi D, Thomas J, Shen Y (2018) The comparative effect of wrapping solid gold nanoparticles and hollow gold nanoparticles with doxorubicin-loaded thermosensitive liposomes for cancer thermo-chemotherapy. Nanoscale 10:8628–8641. https://doi.org/10.1039/C7NR09083H

15. Bhunia SK, Zeiri L, Manna J, Nandi S, Jelinek (2016) Carbon-dot/silver-nanoparticle flexible SERS-active films. ACS Appl Mater Interfaces 8:25637–25643. https://doi.org/10.1021/acsami.6b10945

16. Baker SN, Baker GA (2010) Luminescent carbon nanodots: emergent nanolights. Angew Chem Int Edit 49:6726–6744. https://doi.org/10.1002/anie.200906623

17. Liu JW, Luo Y, Wang YM, Duan LY, Jiang JH, Yu RQ (2016) Graphitic carbon nitride nanosheets-based ratiometric fluorescent probe for highly sensitive detection of H_2O_2 and glucose. ACS Appl Mater Interfaces 8:33439–33445. https://doi.org/10.1021/acsami.6b11207

18. Han M, Wang L, Li S, Liang B, Zhou Y (2017) High-bright fluorescent carbon dot as versatile sensing platform. Talanta 174:265–273. https://doi.org/10.1016/j.talanta2017.05.067

19. Hamd-Ghadareh S, Hamah-Ameen BA, Salimi A, Fath F, Soleimani F (2019) Ratiometric enhanced fluorometric determination and imaging of intracellular microRNA-155 by using carbon dots, gold nanoparticles and rhodamine B for signal amplification. Microchim Acta 186:469. https://doi.org/10.1007/s00604-019-3446-1

20. Dong Y, Shao J, Chen C, Li H, Wang RX, Chi YW, Xiao XM, Chen GN (2012) Blue luminescent graphene quantum dots and graphene oxide prepared by tuning the carbonization degree of citric acid. Carbon 50:4738–4743. https://doi.org/10.1016/j.carbon.2012.06.002

21. Zhou Z, Zhao L, Wang Z, Xue W, Wang Y, Huang Y, Liang J, Chen J, Li G (2018) Colorimetric detection of 1,5-anhydroglucitol based on graphene quantum dots and enzyme-catalyzed reaction. Int J Biol Macromol 112:1217–1224. https://doi.org/10.1016/j.ijbiomac.2018.02.093

22. Kuo SY, Li HH, Wu PJ, Chen CP, Huang YC, Chan YH (2015) Dual colorimetric and fluorescent sensor based on semiconducting polymer dots for ratiometric detection of lead ions in living cells. Anal Chem 87:4765–4771. https://doi.org/10.1021/ac504845t

23. Miao X, Qu D, Yang D, Nie B, Zhao YK, Fan HY, Sun ZC (2018) Synthesis of carbon dots with multiple color emission by controlled graphitization and surface functionalization. Adv Mater 30:1704740. https://doi.org/10.1002/adma.201870002

24. Rejman J, Oberle V, Zuhorn IS, Hoekstra D (2004) Size-dependent internalization of particles via the pathways of clathrin- and caveolae-mediated endocytosis. Biochem J 377:159–169. https://doi.org/10.1042/BJ20031253

25. Pelossof G, Tel-Vered R, Liu XQ, Willner I (2011) Amplified surface plasmon resonance based DNA biosensors, aptasensors, and Hg^{2+} sensors using hemin/G-quadruplexes and Au nanoparticles. Chem Eur J 17:8904–8912. https://doi.org/10.1002/chem.201100601

26. Zong LP, Ruan LY, Li JJ, Robert SM, Wang JS, Cosnier S, Zhang XJ, Shan D (2021) Fe-MOGs-based enzyme mimetic and its mediated electrochemiluminescence for *in situ* detection of H_2O_2 released from Hela cells. Biosens Bioelectron 184:113216. https://doi.org/10.1016/j.bios.2021.113216

27. Mao X, Liu S, Su B, Wang D, Huang Z, Li J, Zhang Y (2020) Luminescent europium(III)-organic framework for visual and on-site detection of hydrogen peroxide via a tablet computer. Microchim Acta 187:416. https://doi.org/10.1007/s00604-020-04379-4

28. Li N, Liu SG, Dong JX, Fan YZ, Ju YJ, Luo HQ, Li NB (2018) Using high-energy phosphate as energy-donor and nucleus growth-inhibitor to prepare carbon dots for hydrogen peroxide related biosensing. Sens Actuators B Chem 262:780–788. https://doi.org/10.1016/j.snb.2018.02.051

29. Mao Z, Qing Z, Qing T, Xu F, Wen L, He X, He D, Shi H (2015) Poly(thymine)-templated copper nanoparticles as a fluorescent indicator for hydrogen peroxide and oxidase-based biosensing. Anal Chem 87:7454–7460. https://doi.org/10.1021/acs.analchem.5b01700

30. Yadav PK, Singh VK, Chandra S, Bano D, Kuma V, Talat M, Hasan SH (2018) Green synthesis of fluorescent carbon quantum dots from Azadirachta indica leaves and their peroxidase-mimetic activity for the detection of H_2O_2 and ascorbic acid in common fresh fruits. ACS Biomater Sci Eng 5:5623–5632. https://doi.org/10.1021/acsbiomaterials.8b01528

31. Cairns RA, Harris IS, Mak TW (2011) Regulation of cancer cell metabolism. Nat Rev Cancer 11:85–95. https://doi.org/10.1038/nrc2981

32. Trachootham D, Alexandre J, Huang P (2009) Targeting cancer cells by ROS-mediated mechanisms: a radical therapeutic approach? Nat Rev Drug Discov 8:579–591. https://doi.org/10.1038/nrd2803